

Extraordinary optical transmission and vortex excitation by periodic arrays of Fresnel zone plates

A. ROSZKIEWICZ and W. NASALSKI*

Institute of Fundamental Technological Research, Polish Academy of Sciences, 5b Adolfa Pawińskiego St., 02-106 Warsaw, Poland

Abstract. Extraordinary optical transmission and good focusing properties of a two-dimensional scattering structure is presented. The structure is made of Fresnel zone plates periodically arranged along two orthogonal directions. Each plate consists of two ring-shaped waveguides supporting modes that match the symmetry of a circularly polarized incident plane wave. High field concentration at the focal plane is obtained with the short transverse and long longitudinal foci diameters. Optical vortex excitation in a paraxial region of the transmitted field is also observed and analysed in terms of cross-polarisation coupling. The structure presented may appear useful in visualization, trapping and precise manipulations of nanoparticles.

Key words: Fresnel zone plates, focusing, cross-polarisation coupling, optical vortices.

1. Introduction

Discovery of extraordinary optical transmission (EOT) in a periodic set of holes drilled in an opaque metal layer [1] stimulated extensive research on high transmission through plasmonic structures [2–15]. Different configurations were proposed like one-dimensional slits [2–4] or two-dimensional structures of rectangular [5] and circular symmetry [6–15], pertaining empty holes [6–7] and coaxial guides [8–11]. In addition, different incident field polarizations – linear [12], circular [13], azimuthal [14] or radial [15] – were taken into account. The goal of the research was to obtain high transmission with possibly a long focus of a short transverse diameter.

On the other hand, manipulations of optical information carried in an optical field amplitude, phase and polarization become also an important issue. Within this range the generation of an orbital angular momentum (OAM) was invented in several different ways, based mainly on direct changes of OAM introduced in the field helical phase fronts, on spin-orbit conversions by enforcing changes in the field spin angular momentum (SAM), or on simultaneous manipulations on both OAM and SAM of vector beam fields [16–21]. The spin-orbit conversion also occurs through the cross-polarization coupling (XPC) in fields of vector beams impinging on planar, transversally homogeneous media interfaces or layered structures [22]. In general, the XPC interactions always exist for beam reflection, refraction and transmission under arbitrary incidence [23], even in cases without the spin-orbit conversion [24].

The goal aimed in this paper is placed within these two areas of interests. Interaction of a monochromatic, circularly polarized plane wave with a two-dimensional periodic array of two-ring Fresnel zone plates (FZPs) is numerically analysed

and graphically described. The case of normal incidence is considered, in parallel to the recent report on EOT through a single-ring coaxial structure [15]. The field intensity, phase and polarisation distribution is discussed in detail, with special attention given to the region near the field focus. The presence of optical vortex excitation, as anticipated by analogy to the analysis given in [22], is checked.

Two distinct phenomena are observed. First of all, as lateral dimensions of the structure (radii of the rings) are chosen accordingly to the FZP rule, efficient focusing of the transmitted field is obtained. The FZP alone focuses the field below the structure, even under the plain incident plane wave. Contrary to the case considered in [15] no additional prefocusing of the optical field is needed. The field focus is characterized by a narrow transverse cross-section and a long longitudinal length. The second effect of the structure appears to be the modification – in a well ordered manner – of the field polarization state, as well as its phase and amplitude distribution. This feature is especially enhanced in the paraxial region close to the field focus. In effect, vortex excitation in the transmitted field exists and is clearly visible. Main characteristics of the vortex field follow those known from the beam XPC interactions with planar layered structures [22].

The paper is organized as follows. Section 2 contains the description of geometry of the FZP structure. The focusing properties of the structure are presented in Sec. 3. The amplitude and polarization distributions in horizontal planes inside and outside the structure are shown in Sec. 4. The excitation of modes in coaxial waveguides of the FZP, the XPC interactions and the presence of optical vortices in the orthogonal – to the incident - field components are discussed. In Sec. 5 field polarization and energy flow distributions are described near the field focus. Finally, Sec. 6 concludes main results of the paper.

*e-mail: wnasal@ippt.pan.pl

2. Geometry of the structure

Geometry of the problem is presented in Fig. 1. The right-circularly polarized (CR) plane wave of wavelength $\lambda = 876$ nm impinges on the infinite, periodic, two-dimensional structure under normal incidence. The structure, surrounded by air, consists of two-ring Fresnel zone plates etched in a lossless perfect electric conductor (PEC) layer with a dielectric constant $\varepsilon_{PEC} = -10^8$. The case of PEC was chosen in this analysis to minimize light interaction between air rings in one FZP and between neighbouring FZPs. No E_z field exists inside the perfect conductor due to the boundary conditions requiring vanishing of the tangent E field component at the PEC boundary. The electric field is confined inside the etched air rings. The periodicity of the structure has no influence on the field inside the neighbouring air rings and should only cause interference in the transmitted field below the structure. Moreover, the comparison of the FZPs etched in real metal (silver) is also presented in Fig. 6 below and main differences in the field distribution between the PEC and silver structures are indicated.

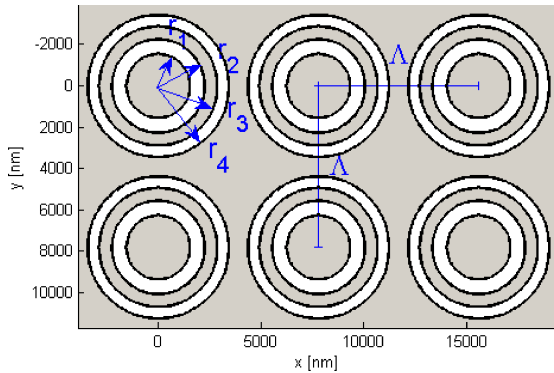


Fig. 1. Geometry of the problem: top view of the two-dimensional periodic structure consisting of two-ring Fresnel zone plates

Accordingly to the Huygens principle, all points in the air rings are considered as sources of secondary spherical waves. Then, the constructive interference in the focal point yields the distance between the edge of each zone and the focal point $R_m = f + m\lambda/2$, where f is the focal length and $m = 1, 2, \dots$. This leads to the equation for the inner and outer radii of each ring in FZP: $r_m = \sqrt{\lambda f m + (\lambda m/2)^2}$, where $m = 1, \dots, 4$ [25]. The focal length is assumed to be $f = 2500$ nm, which gives: $r_{1-4} = 1543, 2269, 2880$ and 3439 nm. Thickness of the structure ($d = 600$ nm) and the limited number of the rings in each FZP slightly move the focus from the theoretical value to $z = 2980$ nm. Periods in x and y directions are equal $\Lambda = 7800$ nm and allow for propagation of $+/- 8$ diffraction orders in air at a given wavelength.

3. Focusing by the structure

Numerical analysis of the optical response of the structure is accomplished by using the rigorous coupled wave analysis [26] adapted to 2D structures [27] with implementation of the scattering matrix algorithm [28] and the factorization

rules [29–31]. In the following calculations 21 diffraction orders in each transverse directions were assumed, which allow for numeric operations on matrices consisting at most of $(4 \cdot 4 \cdot 21 \cdot 21)^2$ elements.

Figure 2 presents the intensity of the total transmitted electric field in the vertical (a) and transverse (b) cross-sections of the focus. The figure confirms that the focusing ability of the structure is high in spite of that it consists only of two air rings. The diameter of the total electric field intensity in the transverse direction at the focal plane, defined as the full width at half maximum (FWHM), is approximately equal to $0.57\lambda \sim 500$ nm. It is lower by 36% than the Rayleigh resolution $R_{Rayl}^{FZP} = 0.61\lambda/NA = 1.22\Delta r_4$ defined here for the FZP consisted of two air rings, which is equal to 682 nm.

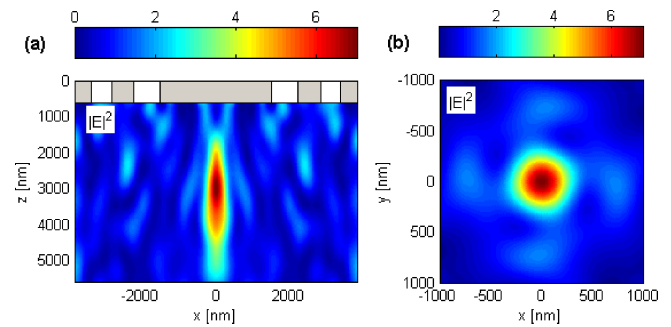


Fig. 2. (a) Side view (cross section at $y = 0$) of the total electric field intensity distribution below the grating with one period visible. (b) Total electric field intensity distribution at the focal plane ($z = 2980$ nm) in the paraxial region

The structure allows also for the large length of the focus in the propagation direction. The focus length, where the electric field intensity does not fall below 50% of its maximum intensity, expressed in the incident wave number k is equal $l_{foc} \approx 2\pi w_w^2/\lambda \approx 448.29k$, which gives 3400 nm. The length of the focus for FZP can be estimated by $l_{foc} = \pm\lambda/\left[2(NA)^2\right] = \pm 2(\Delta r_4)^2/\lambda$ [32]. Here, l_{foc} is defined as a distance from the focal plane, at which the intensity on axis is diminished by 20%. Accordingly to this equation $l_{foc} = \pm 713$ nm. This is slightly larger than numerically calculated (± 630 nm).

Thus, the configuration allows focusing plane wave to sub-wavelength dimensions with the long focal depth at a certain distance from the structure. This configuration does not need former prefocusing of the optical field, as it was applied in [15]. In that case the optical beam was focused before illumination of a single coaxial aperture. The total transmittance, in reference to the transmittance through a glass substrate ($n = 1.5$), was measured. The measured normalized transmittance for radially and azimuthally polarized beam was around 0.45 and 0.08, respectively. Thus the highest measured transmittance corresponds there to highly focused Gaussian beam of radial polarization and is around 0.43. In our configuration, without the need of prefocused of Gaussian beam, the total transmittance through structure is $T = 0.41$ for PEC. The additional difference is the case of circularly polarized plane wave discussed here.

Note that EOT occurs when the normalized-to-area transmittance is larger than unity (Ref. [33]). The case analysed here can be considered as EOT since the normalized-to-area transmittance (defined as the transmission normalized to the amount of light impinging on the area occupied by the air rings) is 1.25.

4. Field spatial distribution

Figure 3 presents the total, transverse and longitudinal electric field intensity distributions in the middle of the structure ($z = 300$ nm), just below the structure ($z = 601$ nm) and at the focal plane ($z = 2980$ nm). The transmitted field consists of the superposition of the waves diffracted from several neighbouring FZPs, but the main output in the vicinity of the z -axis of each FZP structure is originated only from the one FZP placed just above. Moreover, the calculation of amplitudes of the subsequent diffraction orders indicates that the amplitude magnitude of the zero (0,0) transmitted order is at least three times larger than the one of any higher order. Therefore, we are mainly interested in the polarization and phase changes around the axis of each structure, that is,

in the paraxial range near the field focus. Note that the relation between the wavelength and horizontal dimensions of the structure is $2\pi r_i/\lambda > 10$ for each $i = 1, \dots, 4$. Because all of that we present below in the Figs. 4–9 the field and phase distributions only near the FZP axis.

In Fig. 3 strong focusing ability of the structure is revealed for all, the transverse and the longitudinal, field components. The characteristic E_z field distribution with maximum field intensity around the z -axis and zero at the centre is clearly visible not only in the focal plane, but even just below the structure, at $z = 601$ nm.

Regularly placed maxima are visible in the transverse electric field components inside the coaxial rings. They are originated from the superposition of the excited waveguide modes in the structure. Since the normally incident plane wave possesses circular polarization, the symmetry does not allow for basic TEM₀₀ mode excitation [34], the only mode without cut off wavelength in this configuration. Other waveguide modes, to be excited, have to match the symmetry of incident circular polarization and fulfil the boundary conditions. Besides, the amplitude and phase of electric field vector of any mode in real metal needs to fulfil the Bloch theorem. However, in the case of perfect metal, there is no coupling between the cavities and the eigenfrequencies of the modes are independent of the Bloch vector [12]. The dispersion relation that determines the propagation constants of the modes in real metal are presented in Appendix.

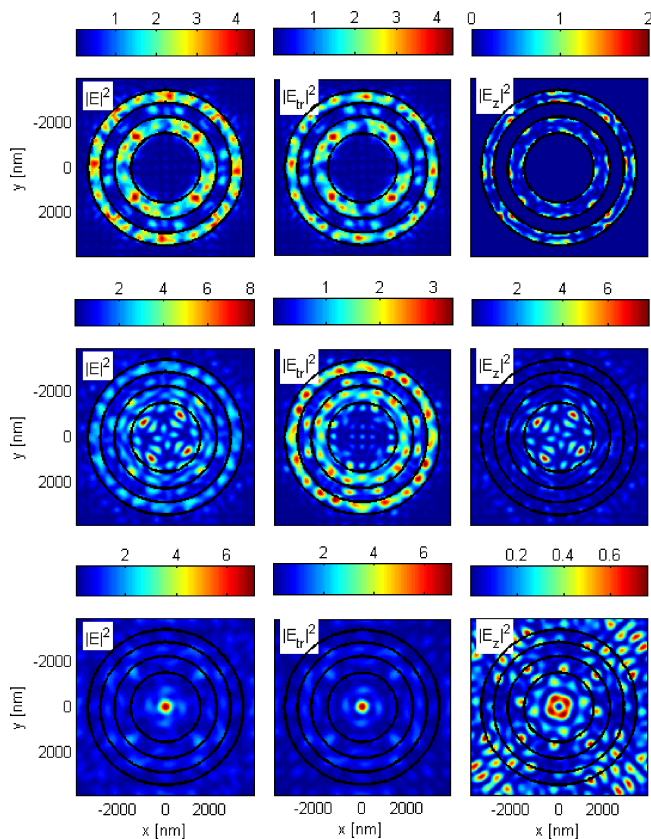


Fig. 3. Electric field intensities; first column: total field, second column: transverse field, third column: longitudinal field. First row: in the middle of the structure at $z = 300$ nm, second row: below the structure at $z = 601$ nm, third row: in the focus at $z = 2980$ nm. The concentric rings of the structure are indicated. As numerical calculations with 21×21 diffraction orders were taken into account, the positions of the maxima around the air rings are evaluated only approximately

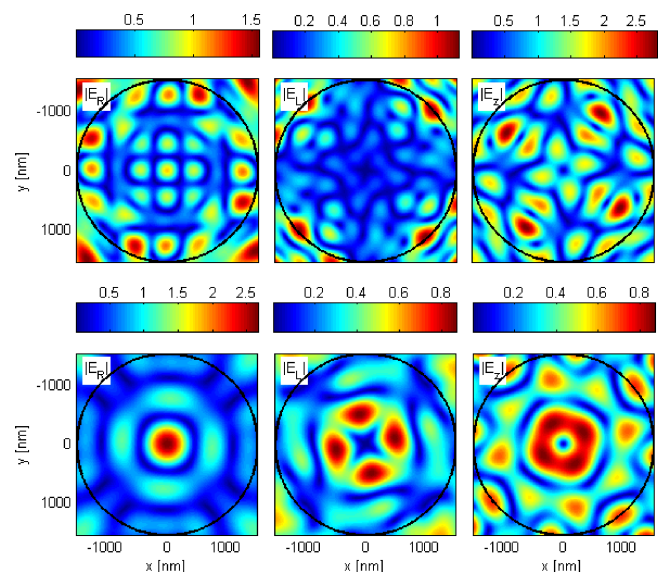


Fig. 4. Absolute amplitude distributions of the transverse $|E_R|$, $|E_L|$ and longitudinal $|E_z|$ electric field components for the structure made of PEC. First row: below the structure ($z = 601$ nm). Second row: at the focal plane ($z = 2980$ nm). Note that only the field in the paraxial region is presented

The modes excited inside the concentric waveguides are rather hybrid modes than the pure TE or TM modes, since both electric and magnetic fields have nonzero longitudinal components $E_z \neq 0$ and $H_z \neq 0$ at each cross-section plane inside the guide. The analytical expressions for the electric

field TE and TM components of the modes and the cut off wavelengths λ^{co} for TE and TM modes in a coaxial waveguide are given in [35]. In the case of the first four modes in the inner and outer rings λ^{co} is approximately equal to: 11976 nm and 19854 nm for TE₁₁ mode, 5988 nm and 9927 nm for TE₂₁ mode, 2279 nm and 1756 nm for TM₁₁ and TM₂₁ modes, respectively. The number of maxima around the outer air ring indicates that also modes of higher indices are excited. These are examples of the modes that match the polarization symmetry of the incident wave and can be excited in this case.

More information about the interaction of the circularly polarized plane wave and the periodic structure made of FZP waveguides can be inferred from the amplitude and phase distributions (Figs. 4 and 5). The amplitude distribution of direct (right circular (CR)) polarization has no sign of optical vortex excitation. The amplitude maxima are placed at the axis and in concentric outer ring, which is additionally modified by the grating periodicity Λ . The influence of neighbouring FZPs can be seen in the area beyond the focus spot. The field pattern indicates the diffraction of the propagating modes at the output of concentric apertures. The cross-polarized (left circular (CL)) and longitudinal components, on the other hand, exhibit the null amplitude at the axis and the outer ring of a maximum amplitude, with four maxima around.

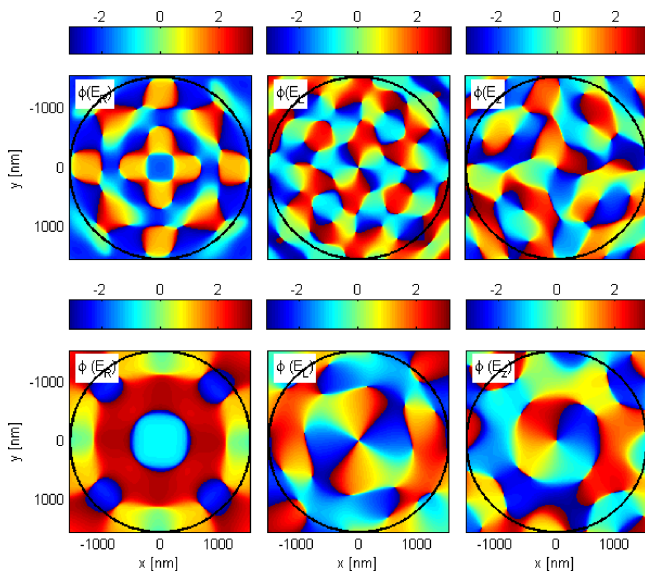


Fig. 5. Phase distributions of the transverse $|E_R|$, $|E_L|$ and longitudinal $|E_z|$ electric field components for the structure made of PEC, corresponding to the amplitude distributions shown in Fig. 4. First row: below the structure ($z = 601$ nm). Second row: at the focal plane ($z = 2980$ nm)

The phase distribution at the focal plane clearly indicates excitation of optical vortices with typical characteristics of the XPC interaction of vector beams of finite cross-sections with a planar layered structure [22]. The vortex of a topological charge equal two is excited (twice 2π -change of phase around the z -axis) in the transverse orthogonally polarized (CL) component and, consequently, also in the longitudinal field component with the topological charge equal one. In

general, in such vortex excitations, the change of the optical topological charge by plus two (minus two) is accompanied by the switch of the field polarisation from CR to CL (CL to CR) in the horizontal plane $z = \text{const}$ [22].

Additionally, the phase of E_z in an outer area around the focus axis is shifted by $\sim \pi$ with respect to the phase of the focus region. Beyond that second phase ring this interference of waves incoming from neighbouring structures influences significantly the field and phase distribution. Similarly, a sharp phase changes at the edges of the focus spot are visible in the direct (CR) and orthogonally polarized (CL) transverse field components.

It was shown in Fig. 6 that the field distribution in real metal (silver with the dielectric function numerically fitted to experimental data [36]) is of the same sort as that described for PEC. Due to possible coupling between the periodically arranged guides in real metal, the presence of neighbouring structures modifies slightly the phase distributions with respect to PEC, particularly visible in the field of direct polarization. Each FZP has four closest-neighbouring FZPs along x and y directions. The four disturbances visible at those directions around FZP indicate that a weak interaction between the closest FZP neighbours really exists.

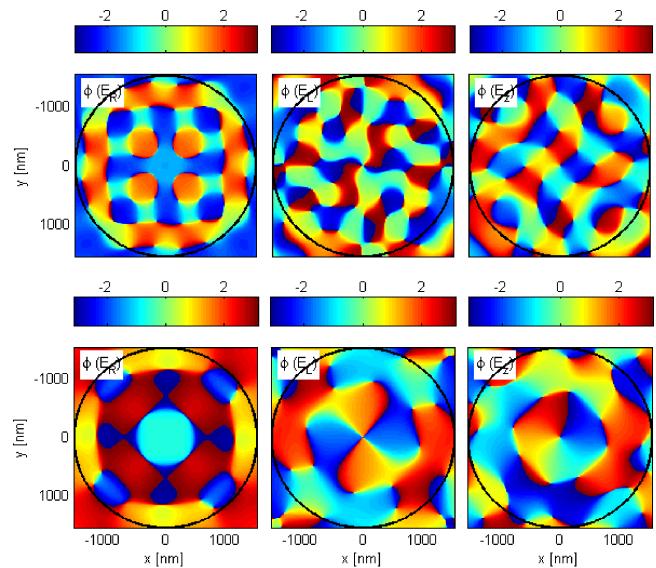


Fig. 6. Phase distributions of the transverse $|E_R|$, $|E_L|$ and the longitudinal $|E_z|$ electric field components for the structure made of silver. First row: just below the structure ($z = 601$ nm). Second row: at the focal plane ($z = 2980$ nm)

The configuration of periodic air holes in the metal layer was also checked. In this case the vortex excitation – although a weak – is also possible. The field focusing, however, is much more pronounced in the case of the FZP structure considered here.

5. Field polarization near focus

As it was numerically verified in Figs. 4–6, the incident plane wave of CR polarization excites the phase singularity in the

orthogonal CL polarization and, consequently, in the longitudinal field component as well. However, the field intensity of the CL field component in the region close to the focus remains in magnitude smaller than that of the CR polarization. Still, it is interesting to see how this excitation influences the polarization distribution of the field near its focus.

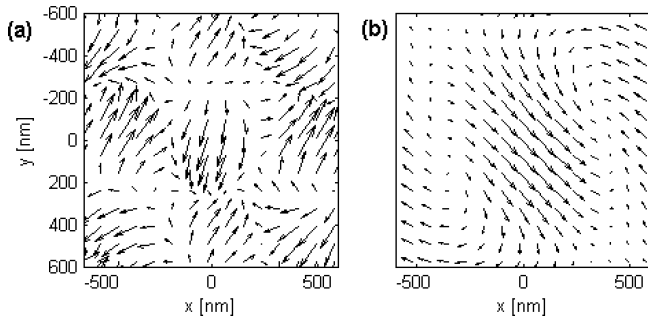


Fig. 7. Transverse real electric field direction just below the structure ($z = 601$ nm) (a) and at the focal plane ($z = 2980$ nm) (b). Note that the field in the paraxial region is only presented

Figure 7 presents the total transverse electric field direction denoted by arrows, just below the structure and in the focal plane. The parallelism of the arrows in the focus corresponds to the dominant right-handed elliptical polarization in paraxial region. The focusing of the field enlarges the range of quasi-homogeneous field polarization. However, the field polarization changes in the transverse plane of the focus. When the polarization vector \underline{A} is decomposed into the x and y polarization components: $\underline{A} = \hat{x}A_x e^{i\delta_x} + \hat{y}A_y e^{i\delta_y}$ with the relative phase $\delta = \delta_y - \delta_x$, then the field in the rotated coordinates x' and y' is described by the ellipse: $(A_{x'}/a)^2 + (A_{y'}/b)^2 = 1$ with the ellipticity $e=b/a$ and the inclination angle $\phi = 2^{-1} \tan^{-1} [2A_x A_y \cos(\delta) / (A_x^2 - A_y^2)]$ [37].

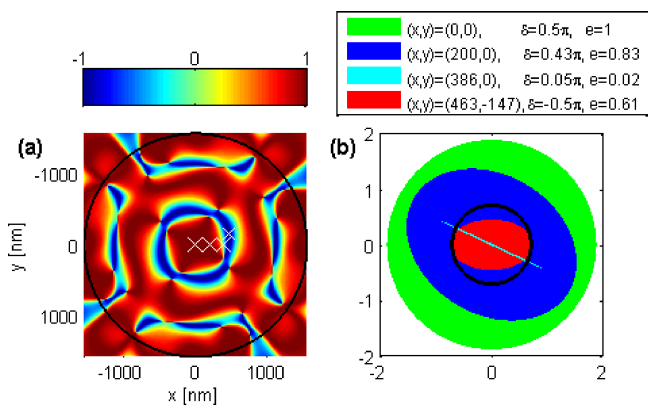


Fig. 8. (a) Values of $\sin\delta$ in the paraxial region of the focal plane, where δ is the phase difference between the two electric field components. (b) Polarization ellipses for four points denoted by crosses in (a). In the legend, subsequent values of δ and the ellipticity e are indicated. The black circle indicates the incident CR wave polarization

Figure 8 describes the field polarization distribution near focus. The electric field polarization changes its handedness several times along the distance from the focus centre, as it

is clearly seen in Fig. 8a. Figure 8b shows the polarization ellipse in the subsequent field points. In the centre point the circular polarization is exactly specified; the outer circle in Fig. 8b corresponds to pure CR polarization at the axis with $\delta = \pi/2$. As the distance from the focus centre grows, the polarization becomes more elliptical (dark-blue and light-blue ellipses) and at the point where $\sin\delta = 0$ the field is linearly polarized. The ring of linearly polarized field around the axis separates the areas where electric field polarization is right- and left-handed, respectively. The red ellipse corresponds to $\sin\delta = -1$, which means the pure left-handed elliptical field.

The changes of the field polarization result in the circular flow of the optical field energy in the first intensity ring around the field focus centre. It is shown in Fig. 9 within the paraxial range of the transmitted field near the focus. Separate regions of maximal values of transverse and longitudinal Poynting vector components confirm the optical vortex excitation in the centre of the beam field.

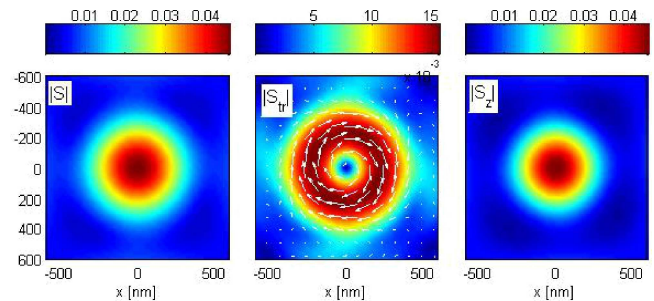


Fig. 9. Amplitudes (colour) and direction (arrows) of the Poynting vector \underline{S} in the focal plane ($z = 2980$ nm); from left to right: the total field, its transverse component and its longitudinal component in the field paraxial region close to the focus centre

6. Conclusions

A new type of a focusing metallic structure is numerically analysed. It consists of the periodically arranged FZPs engraved in perfect electric conductor or silver. The case of normal incidence of a circularly polarized plane wave is considered. The structure allows for extraordinary optical transmission and efficient focusing with no need of prefocusing of the incident field. Moreover, the changes of the field intensity, phase and polarization spatial distribution enforced by the FZP structure indicate the XPC interactions between the polarisation field components [22]. That results in the optical vortex excitation in the orthogonal – to the incident one – polarization field components. The vortex diameter is narrow due to field focusing but still it does not prevail in intensity over the field of incidence polarisation. It seems, however, that the vortex excitation can be made stronger and the focus diameter smaller by using, for example, unidirectional excitations of surface plasmon polaritons at asymmetric nanostructures [38] or other methods typical for metamaterial structures [24, 39]. Due to its properties the FZP structure may appear useful in optical visualization, trapping and precise manipulations of nanoparticles.

Appendix

In the case of a real metal (here silver) the theoretical calculations give the value of the propagation constant equal to 1.0373 in the inner air ring and 1.0484 in the outer air ring for the first TM modes. The calculations rely on the assumption that the propagating mode in each air ring of the coaxial structure has the total wave vector determined by the wave vector for the metal-insulator-metal (MIM) plane cavity [8]: $\beta^2 + k_\theta^2 = \beta_{MIM}^2$. Together with the condition $2\pi r_{ring} k_\theta = 2\pi\nu$ it gives the dispersion relation for an air ring in a coaxial structure:

$$\begin{aligned} & \tanh \left(\sqrt{\beta^2 + \left(\frac{\nu}{r_{ring}} \right)^2 - k_0^2 \varepsilon_d} \frac{d}{2} \right) \\ & + \varepsilon_d \sqrt{\beta^2 + \left(\frac{\nu}{r_{ring}} \right)^2 - k_0^2 \varepsilon_m} \Big/ \\ & \varepsilon_m \sqrt{\beta^2 + \left(\frac{\nu}{r_{ring}} \right)^2 - k_0^2 \varepsilon_d} = 0, \end{aligned} \quad (A1)$$

where $r_{ring} = (r_1 + r_2)/2$ for the inner ring and $r_{ring} = (r_3 + r_4)/2$ for the outer ring, ν is an integer, ε_m and ε_d are permittivities of a metal and a dielectric.

REFERENCES

- [1] T.W. Ebbesen, H.J. Lezec, H.F. Ghaemi, T. Thio, and P.A. Wolff, "Extraordinary optical transmission through sub-wavelength hole arrays", *Nature* 391, 667–669 (1998).
- [2] S. Collin, G. Vincent, R. Haidar, N. Bardou, S. Rommeluere, and J-L. Pelouard, "Nearly perfect Fano transmission resonances through nanoslits drilled in a metallic membrane", *Phys. Rev. Lett.* 104, 027401-1-4 (2010).
- [3] A.T.M.A. Rahman, P. Majewski, and K. Vasilev, "Extraordinary optical transmission: coupling of the Wood-Rayleigh anomaly and the Fabry–Perot resonance", *Opt. Lett.* 37, 1742–4 (2012).
- [4] A. Roszkiewicz and W. Nasalski, "Resonant transmission enhancement at one-dimensional metal gratings", *J. Phys. B: At. Mol. Opt. Phys.* 46, 025401-1-6 (2013).
- [5] D. van Labeke, D. Gerard, B. Guizal, F.I. Baida, and L. Li, "An angle-independent frequency selective surface in the optical range", *Opt. Express* 14, 11945–51 (2006).
- [6] Y. Ekinici, H.H. Solak, and C. David, "Extraordinary optical transmission in the ultraviolet region through aluminum hole arrays", *Opt. Lett.* 32, 172–4 (2007).
- [7] P.B. Catrysse and S. Fan, "Near-complete transmission through subwavelength hole arrays in phonon-polaritonic thin films", *Phys. Rev. B* 75, 075422-1-5 (2007).
- [8] P.B. Catrysse and S. Fan, "Understanding the dispersion of coaxial plasmonic structures through a connection with the planar metal-insulator-metal geometry", *Appl. Phys. Lett.* 94, 231111-1-3 (2009).
- [9] J-S. Bouillard, J. Einsle, W. Dickson, S.G. Rodrigo, S. Carretero-Palacios, L. Martin-Moreno, F.J. Garcia-Vidal, and A.V. Zayats, "Optical transmission of periodic annular apertures in metal film on high-refractive index substrate: the role of the nanopillar shape", *Appl. Phys. Lett.* 96, 201101-1-4 (2010).
- [10] X. Wang, W. Xiong, W. Sun, and Y. Zhang, "Coaxial waveguide mode reconstruction and analysis with THz digital holography", *Opt. Express* 20, 7706–15 (2012).
- [11] F.I. Baida and D. van Labeke, "Light transmission by sub-wavelength annular aperture arrays in metallic films", *Optics Commun.* 209, 17–22 (2002).
- [12] F.I. Baida, D. van Labeke, G. Granet, A. Moreau, and A. Belkhir, "Origin of the super-enhanced light transmission through a 2-D metallic annular aperture array: a study of photonic bands" *Appl. Phys. B* 79, 1–8 (2004).
- [13] J. Wang and W. Zhou, "An annular plasmonic lens under illumination of circularly polarized light", *Plasmonics* 4, 231–235 (2009).
- [14] A. Roberts, "Beam transmission through hole arrays", *Opt. Express* 18, 2528–33 (2010).
- [15] P. Banzer, J. Kindler, S. Quabis, U. Peschel, and G. Leuchs, "Extraordinary transmission through a single coaxial aperture in a thin metal film", *Opt. Express* 18, 10896–904 (2010).
- [16] M. Padgett and L. Allen, "Light with a twist in its tail", *Contemporary Physics* 41, 275–285 (2000).
- [17] M.W. Beijersbergen, L. Allen, H.E.L.O. Van der Veen, and J.P. Woerdman, "Astigmatic laser mode convertes and transfer of orbital angular momentum", *Opt. Commun.* 96, 123–132 (1993).
- [18] M. Stalder and M. Schadt, "Linearly polarized light with axial symmetry generated by liquid-crystal polarization converters", *Opt. Letters* 21, 1948–51 (1996).
- [19] M.A.A. Neil, T. Wilson, and R. Juškaitis, "A wavefront generator for complex pupil function synthesis and point spread function engineering", *J. Microsc.* 197, 219–233 (2000).
- [20] L. Marrucci, E. Karimi, S. Slussarenko, B. Piccirillo, E. Santamato, E. Nagali, and F. Sciarrino, "Spin-to-orbital conversion of the angular momentum of light and its classical and quantum applications", *J. Opt.* 13, 064001-1-13 (2011).
- [21] Z. Zhao, J. Wang, S. Li, and A.E. Willner, "Metamaterials-based broadband generation of orbital angular momentum carrying vector beams", *Opt. Letters* 38, 932–4 (2013).
- [22] W. Nasalski, "Polarization versus spatial characteristics of optical beams at a planar isotropic interface", *Phys. Rev. E* 74, 056613-1-16 (2006).
- [23] W. Nasalski, "Cross-polarized normal mode patterns at a dielectric interface", *Bull. Pol. Ac. Tech.* 58, 141–154 (2010).
- [24] W. Szabelak and W. Nasalski, "Cross-polarization coupling and switching in an open nano-meta-resonator", *J. Phys. B: At. Mol. Opt. Phys.* 44, 215403-1-10 (2011).
- [25] Y. Guo and S.K. Barton, *Fresnel Zone Antennas*, Kluwer Academic Publishers, Dordrecht, 2002.
- [26] M.G. Moharam, E.B. Grann, D.A. Pommet, and T.K. Gaylord, "Formulation for stable and efficient implementation of the rigorous coupled-wave analysis of binary gratings", *J. Opt. Soc. Am. A* 12, 1068–76 (1995).
- [27] H. Kim and B. Lee, "Pseudo-Fourier modal analysis of two-dimensional arbitrarily shaped grating structures", *J. Opt. Soc. Am. A* 25, 40–54 (2008).
- [28] L. Li, "Formulation and comparison of two recursive matrix algorithms for modeling layered diffraction gratings", *J. Opt. Soc. Am. A* 13, 1024–35 (1996).
- [29] L. Li, "Use of Fourier series in the analysis of discontinuous periodic structures", *J. Opt. Soc. Am. A* 13, 1870–1876 (1996).

Extraordinary optical transmission and vortex excitation by periodic arrays of Fresnel zone plates

- [30] G. Granet and B. Guizal, "Efficient implementation of the coupled-wave method for metallic lamellar gratings in TM polarization", *J. Opt. Soc. Am. A* 13, 1019–23 (1996).
- [31] P. Lalanne and G.M. Morris, "Highly improved convergence of the coupled-wave method for TM polarization", *J. Opt. Soc. Am. A* 13, 779–84 (1996).
- [32] Y. Fu, W. Zhou, L.E.N. Lim, C.L. Du, and X.G. Luo, "Plasmonic microzone plate: Superfocusing at visible regime", *Appl. Phys. Lett.* 91, 061124-1-3 (2007).
- [33] S.G. Rodrigo, *Optical Properties of Nanostructured Metallic Systems*, Springer Theses, Springer-Verlag, Berlin, 2012.
- [34] F.I. Baida, "Enhanced transmission through subwavelength metallic coaxial apertures by excitation of the TEM mode", *Appl. Phys. B* 89, 145–149 (2007).
- [35] N. Marcuvitz, *Waveguide Handbook*, Academic Press, New York, 1965.
- [36] B. Johnson and R.W. Christy, "Optical constants of the noble metals", *Phys. Rev. B* 6, 4370–4379 (1972).
- [37] P. Yech, *Optical Waves in Layered Media*, Wiley, New York, 1976.
- [38] A. Roszkiewicz and W. Nasalski, "Unidirectional SPP excitation at asymmetrical two-layered metal gratings", *J. Phys. B: At. Mol. Opt. Phys.* 43, 185401-1-8 (2010).
- [39] K. Kempa and A. Rose, "Negative refraction of photonic and polaritonic waves in periodic structures", *Bull. Pol. Ac. Tech.* 57, 35–38 (2009).